Relative importance of dispersion and rate-limited mass transfer in highly heterogeneous porous media: Analysis of a new tracer test at the Macrodispersion Experiment (MADE) site

Gaisheng Liu,[1] Chunmiao Zheng,[2] Geoffrey R. Tick,[2] James J. Butler Jr.,[1] and Steven M. Gorelick[3]

Received 24 July 2009; revised 6 October 2009; accepted 26 October 2009; published 20 March 2010.

[1] A single-well injection-withdrawal (SWIW) bromide tracer test was conducted to further investigate transport processes at the Macrodispersion Experiment (MADE) site on Columbus Air Force Base in Mississippi. The bromide breakthrough curve is highly asymmetric and exhibits an early time high-concentration peak followed by an extended period of low-concentration tailing. Comparisons of results simulated by advection-dispersion (AD) and dual-domain mass transfer (DDMT) models with the field data show that the DDMT model more accurately represents the magnitudes of both the early high-concentration peak and the later low-concentration tail. For both the AD and DDMT models, the match with field data is enhanced by incorporating hydraulic conductivity information from new direct-push profiling methods. The Akaike information criterion for the DDMT models is much smaller than that for the AD models in both the homogeneous and heterogeneous cases investigated in this work. The improved match of the DDMT model with the SWIW test data supports the hypothesis of mass transfer processes occurring at this highly heterogeneous site.

Citation: Liu, G., C. Zheng, G. R. Tick, J. J. Butler Jr., and S. M. Gorelick (2010), Relative importance of dispersion and rate-limited mass transfer in highly heterogeneous porous media: Analysis of a new tracer test at the Macrodispersion Experiment (MADE) site, *Water Resour. Res.*, *46*, W03524, doi:10.1029/2009WR008430.

1. Introduction

[2] Over the past two decades, the Macrodispersion Experiment (MADE) site on Columbus Air Force Base in Mississippi has been the location of a series of large-scale tracer tests directed at developing a better understanding of solute transport processes in a highly heterogeneous fluvial aquifer [*Zheng*, 2006]. Researchers have proposed various theories and models to explain the observed tracer behavior at the MADE site [*Berkowitz and Scher*, 1998; *Eggleston and Rojstaczer*, 1998; *Zheng and Jiao*, 1998; *Benson et al.*, 2001; *Feehley et al.*, 2000; *Harvey and Gorelick*, 2000; *Julian et al.*, 2001; *Barlebo et al.*, 2004; *Salamon et al.*, 2007; *Liu et al.*, 2008; *Zhang and Benson*, 2008; *Llopis-Alberta and Capilla*, 2009]. Previous studies have shown that the classical macrodispersion model based on flowmeter hydraulic conductivity (K) measurements cannot capture the major plume characteristics, indicating that solute spreading at the MADE site is most likely controlled by rate-limited mass transfer and not macrodispersion [*Feehley et al.*, 2000; *Harvey and Gorelick*, 2000; *Julian et al.*, 2001]. *Barlebo et al.* [2004], however, considered the possibility that the flowmeter K measurements contain systematic errors, so they represented the K field using eight uniform zones whose values were estimated through inverse modeling of the measured hydraulic heads and concentrations. *Barlebo et al.* [2004] and *Hill et al.* [2006] argued that the macrodispersion model is capable of reproducing the basic transport behavior at the site on the basis of these calibrated K values. *Molz et al.* [2006] disagreed, pointing out that the calibrated K values of *Barlebo et al.* [2004] appear too high compared with prior pumping test values and that the model of *Barlebo et al.* [2004] underpredicts the peak tracer concentration by a factor of 8.

[3] To better understand the transport process at the MADE site, we conducted a single-well injection-withdrawal (SWIW) tracer test (referred to as MADE-4). Unlike the previous large-scale tracer experiments [*Boggs et al.*, 1992, 1993], we focused on the effects of small-scale (less than a few meters) mass transfer features, as numerous studies have suggested such features play a critical role in controlling solute transport at the site [e.g., *Berkowitz and Scher*, 1998; *Feehley et al.*, 2000; *Harvey and Gorelick*, 2000; *Zheng and Gorelick*, 2003; *Liu et al.*, 2004]. The SWIW tracer test, sometimes referred to as a push-pull test, involves injecting and withdrawing a tracer at the same well. A resting period occurs between injection and withdrawal to allow the tracer to move into lower K materials. SWIW tests at other sites have been used extensively to determine biochemical properties [e.g., *Istok et al.*, 1997], dispersivities [e.g., *Güven et al.*, 1985], mass transfer rate coefficients [e.g., *Harvey et al.*, 1994; *Haggerty*

[1]Kansas Geological Survey, University of Kansas, Lawrence, Kansas, USA.
[2]Department of Geological Sciences, University of Alabama, Tuscaloosa, Alabama, USA.
[3]Department of Environmental Earth System Science, Stanford University, Stanford, California, USA.

0043-1397/10/2009WR008430

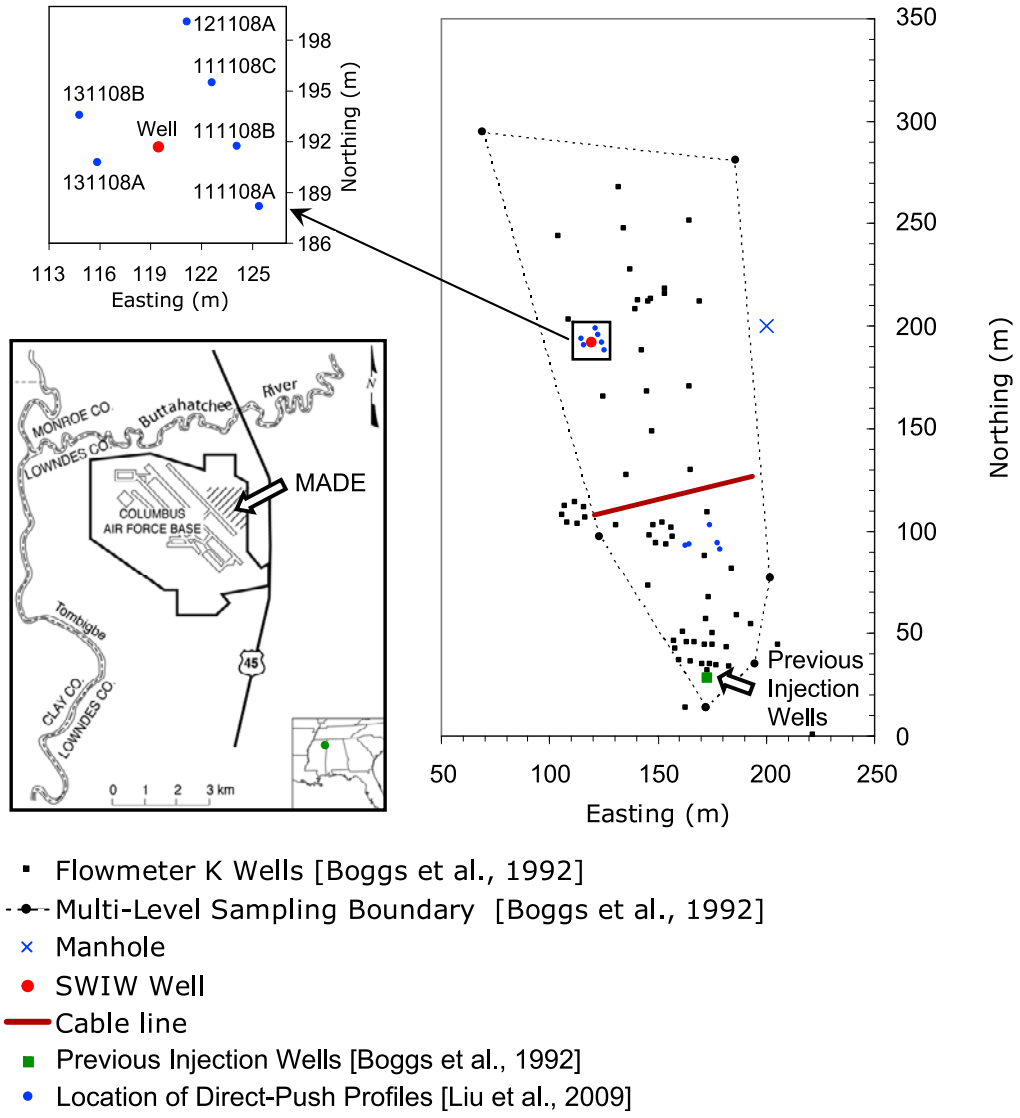

Figure 1. Location of the SWIW test site. The SWIW well is situated 172 m NNW of the source injection wells used in the previous Macrodispersion tracer experiments [*Boggs et al.*, 1992]. The top inset map shows the location of six direct-push profiles in the vicinity of the SWIW well [*Liu et al.*, 2009].

et al., 2001], and other physiochemical characteristics of subsurface media [e.g., *Schroth et al.*, 2001].

2. Experimental Setup and Data

[4] The SWIW test well is located ~172 m NNW of the source injection wells used in the 1992–93 tracer experiments (Figure 1). The well was drilled in 2004 using the mud rotary method. The well is 0.1 m in diameter and 9.75 m deep, with a screened interval 3.66–9.75 m below land surface and a filter pack consisting of commercial well-sorted medium sands. The shallow unconfined aquifer at the site is composed of unconsolidated Pleistocene fluvial terrace deposits that are associated with the nearby Tombigbee and Buttahatchee Rivers (Figure 1). Hydrogeological [*Boggs et al.*, 1992] and geophysical surveys [*Bowling et al.*, 2005] indicate that the major aquifer unit consists of poorly to well-sorted sand and gravel with small amounts of silt and clay. The conductive 6.10–7.62 m thick sand-gravel facies is overlain by ~3 m of clay-rich channel deposits and underlain by fine-grained sands and a clay aquitard of the marine Eutaw formation. Unlike relatively homogeneous field sites, such as those at Borden, Ontario [*Sudicky*, 1986] and Cape Cod, Massachusetts [*LeBlanc et al.*, 1991], the aquifer at the MADE site is highly heterogeneous at a multiplicity of scales [*Rehfeldt et al.*, 1992].

[5] In the SWIW experiment, bromide was used as the conservative tracer. A bromide solution was prepared on site by mixing 1.5 m^3 of extracted groundwater with 1.923 kg of NaBr, yielding a bromide concentration of ~1000 mg/L. A preliminary calculation indicated a relative density of 0.0013 between the bromide source solution and the background groundwater (relative density is defined as the density difference between the bromide solution and native groundwater divided by the density of native groundwater). Given that the average hydraulic gradient is about 0.003 at the site, and the local gradient induced by injection and withdrawal during this test was much larger, density effects

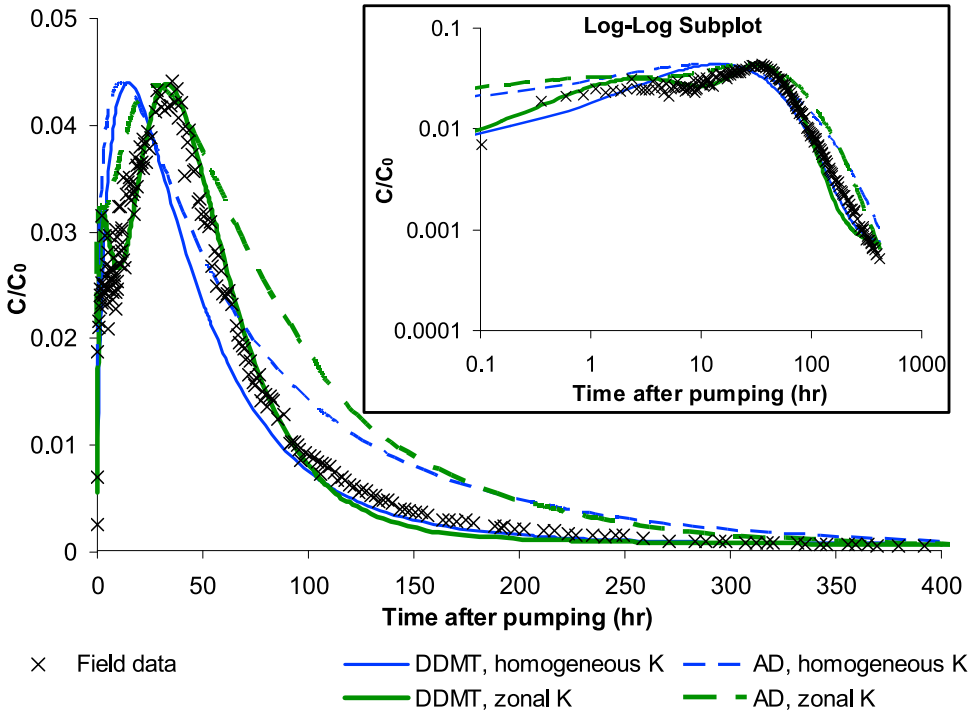

Figure 2. Simulated results for the AD and DDMT models along with the observed data from the SWIW field experiment. Inset shows plots in log-log format. The AD models overshoot the late-time low-concentration tail. The DDMT models better reproduce the magnitudes of both the early peak and late tail.

were deemed to be insignificant during the tracer test [*Barth et al.*, 2001].

[6] The SWIW field experiment can be divided into the following five successive steps: (1) Native water (i.e., site water without tracer) injection for 2.25 h at a rate of 8.18 m^3/d to establish a quasi-steady flow field prior to tracer injection, (2) uniform injection of 1.4 m^3 of bromide solution for 4.1 h at a rate of 8.18 m^3/d, (3) native water injection at 8.18 m^3/d for 24.5 h to push the bromide tracer away from the well, (4) a well shut-in period of 18.7 h to allow bromide to move into lower K materials, and (5) withdrawal of groundwater at 7.90 m^3/d for 410.3 h while collecting water samples in 60 mL Nalgene vials. The withdrawn water was temporarily stored in two 75.7 m^3 storage tanks during the tracer recovery stage (step 5). The vials of tracer samples were placed in ice coolers and transported to the lab where bromide concentrations were measured using ion chromatography (IC) in an ion exchange column. For IC analysis, each sample was subdivided into 5.6 mL analysis vials and loaded onto an autosampler (Dionex ASM-3). Each injection by the autosampler took 2.5 mL of the solution so duplicates of each sample could be obtained for quality control. Bromide concentrations were determined with a Dionex High Performance Ion Chromatograph (Model DX600, Dionex Corp., Sunnyvale, California) equipped with a conductivity detector (Dionex CD25) connected to the autosampler. The column used for the analysis was a Dionex AS14A Anion-Exchange Column (7 mm; 4 × 250 mm; Dionex Corp.), which separates anions by their exchange capacity. Br- was exchanged for hydrogen and the conductivity detector recorded the signal. The lower detection limit was approximately 0.1 mg/L and the coefficient of variation was less than 10% for all measured samples. No bromide was detected in the native groundwater before tracer injection.

[7] Figure 2 shows the bromide tracer concentrations from the SWIW test. Tracer samples (marked by crosses) were collected much more frequently in the earlier period of the test so that the behavior during the high concentration period could be characterized accurately. The bromide breakthrough curve is asymmetric and displays an early time peak followed by an extended period of low-concentration tailing. The peak concentration occurred 35.5 h after withdrawal began. The total observed mass recovery was calculated to be 78.4%, which is comparable with reported recoveries from other SWIW tests [e.g., *Meigs and Beauheim*, 2001].

3. Simulation Analysis

3.1. Governing Equations

[8] A major goal of the SWIW field experiment was to evaluate the efficacy of different models to represent solute transport processes at this location on the heterogeneous MADE site. For this initial analysis, we compare the classical advection-dispersion (AD) and dual-domain mass transfer (DDMT) models and evaluate their relative ability to reproduce the observed SWIW tracer-test data.

[9] The 3-D governing equation for flow through porous media is given as [*Bear*, 1972]

$$\nabla \cdot [K(\boldsymbol{x})\nabla h(\boldsymbol{x},t)] + q_s = S_s \frac{\partial h(\boldsymbol{x},t)}{\partial t}, \qquad (1)$$

where h is hydraulic head, K is hydraulic conductivity, q_s is a fluid sink-source term, S_s is specific storage, $\boldsymbol{x}$ is the

spatial Cartesian coordinate vector (x, y, z), t is time, and ∇ is the gradient operator given by ($\partial/\partial x$, $\partial/\partial y$, $\partial/\partial z$).

[10] The transport of a conservative solute in 3-D groundwater flow subject to advection, dispersion, rate-limited mass transfer and a fluid sink or source can be written as [*Feehley et al.*, 2000]

$$n_m \frac{\partial C_m}{\partial t} + n_{im} \frac{\partial C_{im}}{\partial t} = \nabla \cdot (n_m D \nabla C_m) - \nabla \cdot (q C_m) + q_s C_s, \quad (2a)$$

$$n_{im} \frac{\partial C_{im}}{\partial t} = \xi (C_m - C_{im}), \quad (2b)$$

where C_m and n_m are the concentration and porosity in the mobile domain, C_{im} and n_{im} are the concentration and porosity in the immobile domain, C_s is the concentration of the fluid source-sink flux q_s, D is the hydrodynamic dispersion tensor [*Burnett and Frind*, 1987], q are the components of the specific discharge vector whose values are calculated from the solution of (1), and ξ is the first-order mass transfer rate coefficient between the mobile and immobile fluid domains. The mass transfer process between the mobile and immobile domains is approximated by a single-rate, linear non-equilibrium model. As shown by *Liu et al.* [2007], the bulk mass transfer rate coefficient ξ is controlled by both diffusion and slow advection between the mobile and immobile domains. In the AD approach, where there is no separation of distinct mobile and immobile zones, C_{im} and n_{im} are zero and (2b) does not exist. In the DDMT model, (2a) and (2b) are solved simultaneously to represent a porous medium consisting of mobile and immobile domains where (2a) describes the advective and dispersive processes in the mobile domain and (2b) describes the mass exchange into or out of the mobile domain.

3.2. Numerical Model

[11] To model the SWIW field tracer experiment, (1) and (2) were solved numerically in a 3-D domain 158 m long by 158 m wide by 7.62 m thick centered on the test well using the flow and transport codes MODFLOW-2000 [*Harbaugh et al.*, 2000] and MT3DMS [*Zheng and Wang*, 1999], respectively. The simulation domain was discretized into 201 columns, 201 rows and 25 layers. All layers were of uniform thickness (0.305 m). Within each layer, a horizontal grid spacing of 0.305 m by 0.305 m was used in the vicinity of the test well and the spacing gradually expanded away from the well. Hydraulic boundary conditions are zero gradient across the top and bottom, and constant head (7.47 m above horizontal aquifer bottom) on the four lateral boundaries, which are each ~79 m from the test well. The specific yield of the sand-gravel facies in the test area was determined to be 0.1 [*Boggs et al.*, 1992]. The confined storage coefficient is estimated to be 1.0×10^{-5}. Initial simulations indicated that the ambient average hydraulic gradient of ~0.003, which was small compared to the local gradient created by the SWIW test, had a minimal effect during the tracer test. As a result, the ambient gradient is neglected in the following simulation analysis.

[12] Two different hydraulic conductivity configurations were explored: (1) A homogenous case in which the K was assigned a constant value of 5.27 m/d on the basis of a pumping test conducted at the test well, and (2) a zonal heterogeneous case in which three different K zones were used in an effort to further improve the match to the arrival time of the concentration peak (Figure 3).

[13] A molecular diffusion coefficient of 8.0×10^{-5} m^2/d was used for bromide in the transport simulations [*Harvey and Gorelick*, 2000]. The longitudinal dispersivity value was calibrated by matching to the concentration data. The transverse and vertical dispersivities were fixed at 0.01 and 0.001, respectively, of the longitudinal dispersivity estimate on the basis of previous studies [*Feehley et al.*, 2000]. The dispersivities are assumed not to be changing with time during a simulation.

[14] In the AD model, only a single porosity is used. This porosity has been commonly referred to as "effective porosity," which is often a fitting parameter used to account for dual-porosity effects in a single-porosity context [*Zheng and Bennett*, 2002]. In this study, we explored many effective porosity values for the AD model in an attempt to achieve the best match between the simulated and measured breakthrough curves. The results obtained using the AD model shown in Figure 2 are based on a porosity value of 0.044, which is also the calibrated value of the mobile porosity in the DDMT model. Additional simulations (not reported here) showed that the overall AD model match was not improved when using a different effective porosity value.

[15] Compared with the AD approach where the longitudinal dispersivity is the only parameter to calibrate, the DDMT model requires two additional parameters, the mass transfer rate coefficient, ξ, and the mobile porosity ratio, $\Phi = n_m/(n_m + n_{im})$. Here $(n_m + n_{im})$ is the total porosity and set equal to 0.35 based on core measurements and the possibility of consolidation during handling of core samples [*Boggs et al.*, 1992; *Adams and Gelhar*, 1992]. The mobile and immobile porosities are then calculated as $n_m = 0.35 \times \Phi$ and $n_{im} = 0.35 \times (1 - \Phi)$, respectively. In the DDMT model, Φ, ξ and the longitudinal dispersivity were all adjusted to match the concentration data from the SWIW experiment.

[16] The SWIW test well is at the center of the model domain with the screen extending over layers 1–20 and the pumping/injection rate proportionally distributed according to the K value of each layer intersecting the screen (all layers have uniform thickness). In accordance with the SWIW field procedure, five stress periods were used in the flow and transport simulations. The first three stress periods consisted of 2.25 h of native water injection, 4.1 h of 1000 mg/L tracer injection, and 24.5 h of native water injection, all with a constant injection rate of 8.18 m^3/d. The fourth stress period was a shut-in (no injection or withdrawal) period of 18.7 h. The fifth stress period consisted of the continuous withdrawal of tracer water at 7.90 m^3/d for 410.3 h. In the first three stress periods, flow from the well into the aquifer occurred through the entire screened interval, i.e., all 20 model layers that intersect the well screen. In the fifth stress period, however, because of the drawdown at the well, the effective screen length is reduced to 4.57 m, extending from layer 6 to 20. The first three stress periods are approximated as steady state in the flow model (i.e., $\partial h/\partial t = 0$ in equation (1)) because field measurements indicated that hydraulic heads became stable during the native water injection in the first period, and the actual tracer solution was not introduced until the second period when the flow field was quasi-steady. Transient flow

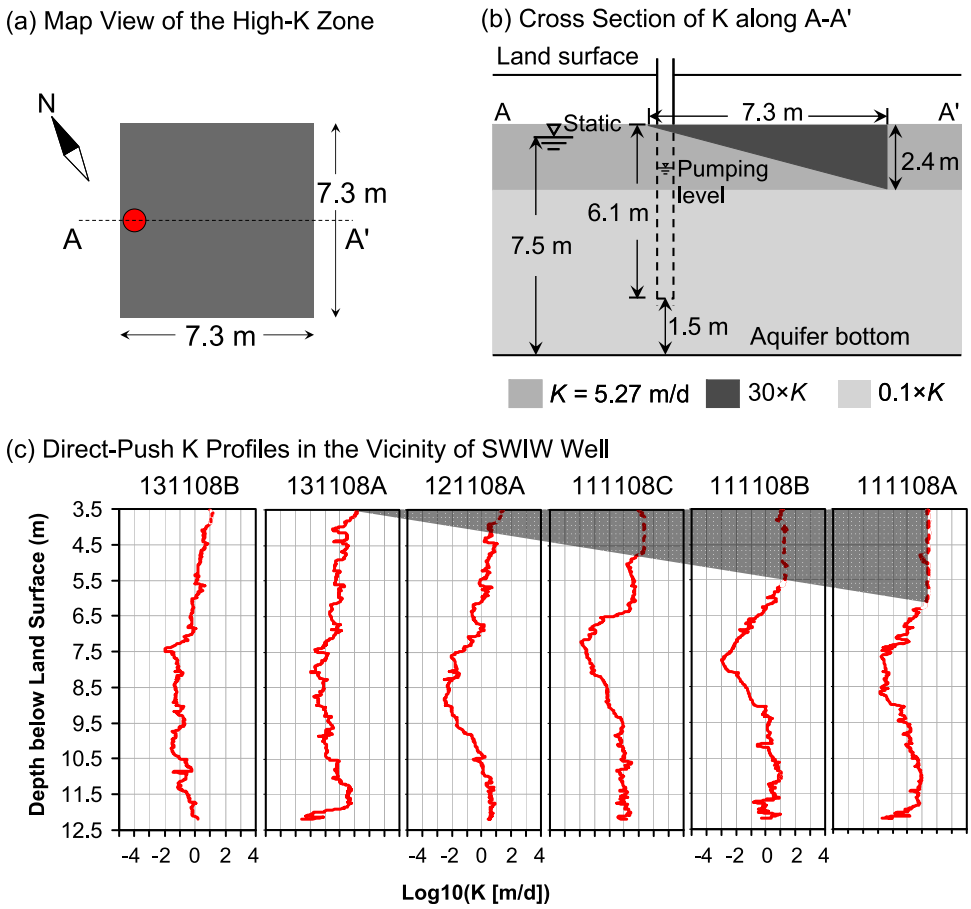

Figure 3. Schematic of the three-zone heterogeneous K field that is based on a series of direct-push K profiles obtained in the vicinity of the test well [*Liu et al.*, 2009]: (a) map view, (b) cross section of K, and (c) direct-push K profiles. The location of the direct-push profiles is in Figure 1. The K in the lower part of the aquifer is set one order of magnitude smaller than the value used in the homogeneous case, while there is a local wedge-shaped high-K zone in the upper part of the aquifer as indicated by the shaded area in Figure 3c. Dashed lines in Figure 3c indicate zones where K exceeds 10 m/d. Note that the water level in the well rose above the top of the screen during injection and quickly dropped 1.5 m after pumping started (pumping and static levels marked in Figure 3b). Diagrams are not to scale.

was simulated during the fourth and fifth periods to represent the water table decline after injection was shut off and withdrawal began.

3.3. Comparative Model Evaluation Criteria

[17] Visual and statistical comparisons are made between the model simulations of bromide concentrations and the concentration data from the SWIW field test. Because we are interested in the transport behavior through the entire experiment, the logarithms of concentrations are used in the comparison so that the late-time low-concentration tail is given as much weight as the early high-concentration peak. This is particularly pertinent at the MADE site where the extensive low-concentration plume front has proven to be a key feature in previous studies [*Berkowitz and Scher*, 1998; *Benson et al.*, 2001; *Feehley et al.*, 2000; *Harvey and Gorelick*, 2000].

[18] To assess the relative importance of transport processes (e.g., dispersion versus rate-limited mass transfer), we used both visual comparison of plots and a quantitative comparison based on the Akaike information criterion (AIC) [*Burnham and Anderson*, 2004]:

$$\mathrm{AIC} = 2k + N\ln(\mathrm{RSS}/N), \tag{3a}$$

where k is the number of parameters to be adjusted in the transport model (one in the AD model and three in the DDMT model), N is the number of bromide measurements (204, all samples shown in Figure 2 included in computing AIC), and RSS is sum of squares of residuals between ln simulated and ln observed relative concentrations:

$$\mathrm{RSS} = \sum_{i=1}^{N}\left[\ln[C(1,i)/C_0] - \ln[C(2,i)/C_0]\right]^2, \tag{3b}$$

where $C(1, i)$ is the simulated bromide concentration at the pumping well during the recovery stage; $C(2, i)$ is the observed bromide concentration at the pumping well during the recovery stage; i is the time at which the tracer concentration is observed in the SWIW test; and C_0 is the bromide source concentration (1000 mg/L). Note that the AIC not only measures the goodness of fit between the simulated and

Table 1. Summary of the AD and DDMT Model Parameters and AIC for This Study[a]

Model	α_L[b] (m)	Φ	ξ (d^{-1})	AIC
		Homogeneous K		
AD	1.52	NA	NA	−283
DDMT	0.61	1/8	0.005	−527
		Zonal K		
AD	1.07	NA	NA	−294
DDMT	0.20	1/8	0.005	−588

[a]NA means not applicable.
[b]Longitudinal dispersivity estimates; transverse and vertical dispersivities are fixed at 0.01 and 0.001, respectively, of longitudinal dispersivity.

observed concentrations, but also takes into account model complexity through a penalty term for the number of adjustable parameters. When the calculated AIC for a model is smaller, that model is considered to be a more appropriate representation of tracer transport during our SWIW field experiment.

4. Results and Discussion

4.1. Homogenous *K*

[19] Figure 2 shows the results of the AD and DDMT modeling analyses in which hydraulic conductivity is assumed homogenous. The calibrated model parameter values are listed in Table 1. The calibrated longitudinal dispersivity value was smaller in the DDMT model than in the AD model, indicating that the role of dispersion is reduced after the mass transfer process is incorporated. The simulated radius of tracer movement from the pumping well (assuming a detection concentration limit of 0.1 mg/L) was 7.9 m in the DDMT model and 10.1 m in the AD model. It is noteworthy that the simulated tracer movement for the AD model is based on a porosity value of 0.044, the same as the mobile porosity for the DDMT model. Using different porosity values for the AD model affects the tracer movement (as the effective pore water velocity will change), but does not improve the match with the observed breakthrough data at the well. This is because when K is homogenous, tracer movement during the SWIW test is balanced out between the injection and withdrawal phases (tracer going out quicker will come back to the well quicker). Additional simulations indicated that both the AD and DDMT model results were not affected by changing the effective K value, as simulated tracer movement was determined by the injection/withdrawal rates that remained constant in the field.

[20] To evaluate the sensitivity of results to estimates of different model parameters, we compute the sensitivity of breakthrough concentrations with respect to each parameter p:

$$RS_p = \sqrt{\frac{1}{N}\sum_{i=1}^{N}\left(\frac{\partial \ln(C_i/C_0)}{\partial p/\hat{p}}\right)^2}, \quad (4)$$

where ∂p is the small perturbation around the calibrated parameter value $\hat{p}$ and $\partial\ln(C_i/C_0)$ is the change in the ln model-simulated breakthrough concentration (normalized by source concentration) at observation time i. Table 2 lists the relative sensitivities of different parameters (dimensionless) in the AD and DDMT models computed using the parameter estimation package, PEST [*Doherty*, 2004]. Table 2 indicates that in the DDMT model, the simulated breakthrough concentrations are least sensitive to the mobile porosity ratio.

[21] Figure 2 indicates that while the AD model successfully reproduces the magnitudes of high concentrations in the early part of the bromide breakthrough curve in the homogeneous case, it significantly overshoots the low-concentration tail at late times. The DDMT model, on the other hand, provides a closer match to both the magnitudes of the early high-concentration peak and the late low-concentration tail. The simulated mass recovery is 95.4% in the AD model, as compared to 68.6% in the DDMT model, indicating that the simulated tail in the AD model would quickly diminish if pumping were to have continued as most mass was already recovered at the end of the simulation. The mass recovery in the DDMT model is closer to that observed in the field (78.4%), so the simulated tail in the DDMT model would be maintained for a period of time if pumping were to have continued. The calculated AIC for the DDMT model is −527, significantly smaller than −283 in the AD model, suggesting that rate-limited mass transfer is playing an important role at the MADE site.

[22] There is a large mismatch between the peak arrival time of the observations and that calculated by the AD and DDMT models in the homogeneous case. The observed peak concentration arrived ~35.5 h after the start of the tracer recovery, but the simulated concentration peaks occur after only 11.4 and 14.6 h in the AD and DDMT models, respectively. In the following section, we consider a zonal K field, coupled with drawdown in the SWIW well, as a plausible explanation for the later peak arrival time observed in the field.

4.2. Zonal *K*

[23] Figure 3 shows the schematic diagram of a simple zonal heterogeneous hydraulic conductivity field that was used in an effort to further improve the match between the observed and simulated arrival times of peak concentrations. This zonal arrangement was based on the results from a series of direct-push K profiles obtained in the vicinity of the test well [*Liu et al.*, 2009], shown in Figure 3c. The K in the lower part of the aquifer was set one order of magnitude smaller than the K used in the homogenous simulations. In addition, there is a wedge-shaped high-K zone in the upper part of the aquifer with the K value set 30 times higher than that used in the homogenous simulations. This high-K wedge, which was observed on the direct-push profiles, pinches out near the top of the well screen and thickens

Table 2. The Relative Sensitivities of Breakthrough Concentrations With Respect to the Calibrated Parameters in the AD and DDMT Models[a]

Model	α_L	Φ	ξ
	Homogeneous K		
AD	0.435	NA	NA
DDMT	0.316	0.149	0.490
	Zonal K		
AD	3.112	NA	NA
DDMT	2.965	0.468	2.549

[a]Sensitivities are dimensionless. NA means not applicable.

away from the well (Figure 3b). The high-K pattern identified here is assumed to be a localized feature that exists only in the immediate vicinity of the SWIW well. The zonal K values, which are consistent with the direct-push profiles (Figure 3c), were determined through preliminary simulations by matching the observed peak arrival time.

[24] During tracer injection, the flow rate into each layer was proportional to the K value of that layer. Thus, a significant amount of mass was introduced into the local high-K layer intersecting the top portion of the screened interval and transported into the nearby high-K zone to the southeast. During pumping, however, there was a rapid 1.5 m drawdown in the well so the high-K zone became disconnected from the well (Figure 3b). As a result, different flow pathways were experienced by the tracer mass in the high-K zone between the injection and recovery stages. This likely caused the delay in the peak arrival time that could not be accounted for by the homogeneous models. It should be emphasized that the three-zone K structure represents merely one of many possible scenarios that could be used to investigate the impacts of heterogeneity on tracer peak arrival time observed in our experiment, but it is consistent with the results of high-resolution direct-push profiling at the site [*Liu et al.*, 2009].

[25] Figure 2 displays the results of the AD and DDMT modeling analyses after the three-zone K field is incorporated. Clearly, the peak arrival time is now represented much better by the DDMT model. The peak arrival time of the AD model also improves, but to a lesser degree. Note that in the DDMT model, the differences in simulation results between the homogeneous- and zonal-K cases mainly occur during the early part of the breakthrough curve. The simulated tails are relatively unaffected by the change in the K structure. The simulated mass recovery is 96.6% in the AD model, as compared to 71.2% in the DDMT model. The simulated tracer movement in the direction of the high-K zone is 12.5 and 14.6 m in the DDMT and AD models, respectively. Compared to those in the homogeneous case, the dispersivity values decrease in both the AD and DDMT models when heterogeneity in K is taken into account (Table 1). The DDMT model-specific parameter estimates, on the other hand, do not change between the homogenous- and zonal-K cases. This indicates that while the peak arrival time appears to be controlled by the K pattern shown in Figure 3, the late-time behavior of the breakthrough curve is primarily controlled by smaller-scale mass transfer processes. Consistent with that idea is the fact that in the zonal-K case, the AD model can simulate the peak concentration, but greatly overshoots the low-concentration tail. By contrast, the DDMT model is able to reasonably represent both parts of the concentration breakthrough curve. The calculated AIC for the DDMT model is −589, much lower than the −294 in the AD model. The improved match of the DDMT model with the SWIW data in both the homogeneous and zonal-K cases suggests the likely occurrence of mass transfer processes at the MADE site.

5. Summary and Conclusions

[26] A SWIW bromide tracer test (MADE-4) conducted at the MADE site provides additional evidence of rate-limited mass transfer in highly heterogeneous media. Unlike the previous large-scale tracer experiments [*Boggs et al.*, 1992, 1993; *Zheng*, 2006], the scale of this new test is relatively small as we focus on the small-scale mass transfer features that are believed to exert a critical role in controlling solute spreading behavior at the site [*Berkowitz and Scher*, 1998; *Feehley et al.*, 2000; *Harvey and Gorelick*, 2000; *Julian et al.*, 2001; *Zheng and Gorelick*, 2003; *Liu et al.*, 2004]. The bromide breakthrough curve from the SWIW experiment is asymmetric and shows an early time peak followed by an extended period of low-concentration tailing.

[27] By comparing the AD and DDMT models to the field data, our results indicate that the AD model can reproduce the magnitudes of high concentrations in the early part of the bromide breakthrough curve, but it significantly overshoots the low-concentration tail at late times. The DDMT model provides a more accurate representation of the magnitudes of both the early high-concentration peak and the late low-concentration tail. The observed peak arrival time could not be reproduced by the AD and DDMT models when the hydraulic conductivity field is considered to be homogenous. A three-zone K structure, which was based on the results of high-resolution direct-push profiling [*Liu et al.*, 2009], was found to significantly improve the match between the observed and simulated peak arrival times. The AIC calculated for the DDMT model is smaller than that for the AD model in both the homogeneous and zonal-K cases examined here, demonstrating that the DDMT model is more appropriate than the AD model for representing the tracer behavior observed in our field test. The improved match of the DDMT model with the SWIW data suggests the possibility of mass transfer processes at the MADE site.

[28] **Acknowledgments.** This material is based upon work supported by the National Science Foundation under grants EAR 0538011, EAR 0537668, EAR 0738960, and EAR-0738955. Any opinions, findings, and conclusions or recommendations expressed in this material are those of the authors and do not necessarily reflect the views of the National Science Foundation. We are grateful to Joe Chandler, Erika Rincon, Jie Liu, and Elizabeth Graham, who provided tremendous assistance in field test setup, sampling and lab analysis, and Troy Stewart, Miranda Brannon, and Mike Smith at the Columbus Air Force Base, who provided aid in gaining access to the MADE site. We also thank Scott Tyler, Tom Torgersen, Alberto Bellin, Fred Molz, and anonymous reviewers whose constructive comments have led to a significant improvement of this paper.

References

Adams, E. E., and L. W. Gelhar (1992), Field study of dispersion in a heterogeneous aquifer: 2. Spatial moment analysis, *Water Resour. Res.*, *28*, 3293–3307, doi:10.1029/92WR01757.

Barlebo, H. C., M. C. Hill, and D. Rosbjerg (2004), Investigating the Macrodispersion Experiment (MADE) site in Columbus, Mississippi, using a three-dimensional inverse flow and transport model, *Water Resour. Res.*, *40*, W04211, doi:10.1029/2002WR001935.

Barth, G. R., T. H. Illangasekare, M. C. Hill, and H. Rajaram (2001), A new tracer-density criterion for heterogeneous porous media, *Water Resour. Res.*, *37*, 21–31, doi:10.1029/2000WR900287.

Bear, J. (1972), *Dynamics of Fluids in Porous Media*, Dover, New York.

Benson, D. A., R. Schumer, M. M. Meerschaert, and S. W. Wheatcraft (2001), Fractional dispersion, Levy motion and the MADE tracer tests, *Transp. Porous Media*, *42*, 211–240, doi:10.1023/A:1006733002131.

Berkowitz, B., and H. Scher (1998), Theory of anomalous chemical transport in fracture networks, *Phys. Rev. E*, *57*(5), 5858–5869, doi:10.1103/PhysRevE.57.5858.

Boggs, J. M., S. C. Young, L. M. Beard, L. W. Gelhar, K. R. Rehfeldt, and E. E. Adams (1992), Field study of dispersion in a heterogeneous aquifer: 1. Overview and site description, *Water Resour. Res.*, *28*, 3281–3291, doi:10.1029/92WR01756.

Boggs, J. M., L. M. Beard, S. E. Long, M. P. McGee, W. G. MacIntyre, C. P. Antworth, and T. B. Stauffer (1993), Database for the Second

Macrodispersion Experiment (MADE-2), *Tech. Rep. TR-102072*, Electr. Power Res. Inst., Palo Alto, Calif.

Bowling, J. C., A. B. Rodriguez, D. L. Harry, and C. Zheng (2005), Delineating alluvial aquifer heterogeneity using resistivity and GPR data, *Ground Water*, *43*(6), 890–903.

Burnett, R. D., and E. O. Frind (1987), An alternating direction Galerkin technique for simulation of groundwater contaminant transport in three dimensions: 2. Dimensionality effects, *Water Resour. Res.*, *23*, 695–705, doi:10.1029/WR023i004p00695.

Burnham, K. P., and D. R. Anderson (2004), Multimodel inference: Understanding AIC and BIC in model selection, *Sociol. Methods Res.*, *33*, 261–304, doi:10.1177/0049124104268644.

Doherty, J. (2004), *PEST—Model-Independent Parameter Estimation*, Watermark Numer. Comput., Australia.

Eggleston, J., and S. Rojstaczer (1998), Identification of large-scale hydraulic conductivity trends and the influence of trends on contaminant transport, *Water Resour. Res.*, *34*, 2155–2168, doi:10.1029/98WR01475.

Feehley, C. E., C. Zheng, and F. J. Molz (2000), A dual-domain mass transfer approach for modeling solute transport in heterogeneous porous media, application to the MADE site, *Water Resour. Res.*, *36*, 2051–2515, doi:10.1029/2000WR900148.

Güven, O., R. W. Falta, F. J. Molz, and J. G. Melville (1985), Analysis and interpretation of single-well tracer tests in stratified aquifers, *Water Resour. Res.*, *21*, 676–684, doi:10.1029/WR021i005p00676.

Haggerty, R., S. W. Fleming, L. C. Meigs, and S. A. McKenna (2001), Tracer tests in a fractured dolomite: 2. Analysis of mass transfer in single-well injection-withdrawal tests, *Water Resour. Res.*, *37*, 1129–1142, doi:10.1029/2000WR900334.

Harbaugh, A. W., E. R. Banta, M. C. Hill, and M. G. McDonald (2000), MODFLOW-2000, the U.S. Geological Survey Modular Ground-Water Model—User guide to modularization concepts and the ground-water flow processes, *U.S. Geol. Surv. Open File Rep., 00-92*, 121 pp.

Harvey, C. F., and S. M. Gorelick (2000), Rate-limited mass transfer or macrodispersion: Which dominates plume evolution at the Macrodispersion Experiment (MADE) site?, *Water Resour. Res.*, *36*, 637–650, doi:10.1029/1999WR900247.

Harvey, C. F., R. Haggerty, and S. M. Gorelick (1994), Aquifer remediation: A method for estimating mass transfer rate coefficients and an evaluation of pulsed pumping, *Water Resour. Res.*, *30*, 1979–1991, doi:10.1029/94WR00763.

Hill, M. C., H. C. Barlebo, and D. Rosbjerg (2006), Reply to comment by F. Molz et al. on "Investigating the Macrodispersion Experiment (MADE) site in Columbus, Mississippi, using a three-dimensional inverse flow and transport model," *Water Resour. Res.*, *42*, W06604, doi:10.1029/2005WR004624.

Istok, J. D., M. D. Humphrey, M. H. Schroth, M. R. Hyman, and K. T. O'Reilly (1997), Single well push-pull test for *in situ* determination of microbal activities, *Ground Water*, *35*(4), 619–631, doi:10.1111/j.1745-6584.1997.tb00127.x.

Julian, H. E., J. M. Boggs, C. Zheng, and C. E. Feehley (2001), Numerical simulation of a natural gradient tracer experiment for the Natural Attenuation Study: Flow and physical transport, *Ground Water*, *39*(4), 534–545, doi:10.1111/j.1745-6584.2001.tb02342.x.

LeBlanc, D. R., S. P. Garabedian, K. M. Hess, L. W. Gelhar, R. D. Quadri, K. G. Stollenwerk, and W. W. Wood (1991), Large-scale natural gradient tracer test in sand and gravel, Cape Cod, Massachusetts: 1. Experimental design and observed tracer movement, *Water Resour. Res.*, *27*, 895–910, doi:10.1029/91WR00241.

Liu, G., C. Zheng, and S. M. Gorelick (2004), Limits of applicability of the advection-dispersion model in aquifers containing connected high-conductivity channels, *Water Resour. Res.*, *40*, W08308, doi:10.1029/2003WR002735.

Liu, G., C. Zheng, and S. M. Gorelick (2007), Evaluation of the applicability of the dual-domain mass transfer model in porous media containing connected high-conductivity channels, *Water Resour. Res.*, *43*, W12407, doi:10.1029/2007WR005965.

Liu, G., Y. Chen, and D. Zhang (2008), Investigation of flow and transport processes at the MADE site using ensemble Kalman filter, *Adv. Water Resour.*, *31*(7), 975–986, doi:10.1016/j.advwatres.2008.03.006.

Liu, G., J. J. Butler Jr., G. C. Bohling, E. Reboulet, S. Knobbe, and D. W. Hyndman (2009), A new method for high-resolution characterization of hydraulic conductivity, *Water Resour. Res.*, *45*, W08202, doi:10.1029/2009WR008319.

Llopis-Alberta, C., and J. E. Capilla (2009), Gradual conditioning of non-Gaussian transmissivity fields to flow and mass transport data: 3. Application to the Macrodispersion Experiment (MADE-2) site, on Columbus Air Force Base in Mississippi (USA), *J. Hydrol.*, *371*(1–4), doi:10.1016/j.jhydrol.2009.03.016.

Meigs, L. C., and R. L. Beauheim (2001), Tracer tests in a fractured dolomite: 1. Experimental design and observed tracer recoveries, *Water Resour. Res.*, *37*, 1113–1128, doi:10.1029/2000WR900335.

Molz, F. J., C. Zheng, S. M. Gorelick, and C. F. Harvey (2006), Comment on "Investigating the Macrodispersion Experiment (MADE) site in Columbus, Mississippi, using a three-dimensional inverse flow and transport model" by H. C. Barlebo, C. Mary Hill, and D. Rosbjerg, *Water Resour. Res.*, *42*, W06603, doi:10.1029/2005WR004265.

Rehfeldt, K. R., J. M. Boggs, and L. W. Gelhar (1992), Field study of dispersion in a heterogeneous aquifer: 3. Geostatistical analysis of hydraulic conductivity, *Water Resour. Res.*, *28*, 3309–3324, doi:10.1029/92WR01758.

Salamon, P., D. Fernandez-Garcia, and J. J. Gómez-Hernández (2007), Modeling tracer transport at the MADE site: The importance of heterogeneity, *Water Resour. Res.*, *43*, W08404, doi:10.1029/2006WR005522.

Schroth, M. H., J. D. Istok, and R. Haggerty (2001), In situ evaluation of solute retardation using single-well push-pull tests, *Adv. Resour. Res.*, *24*, 105–117, doi:10.1016/S0309-1708(00)00023-3.

Sudicky, E. A. (1986), A natural gradient experiment on solute transport in a sand aquifer: Spatial variability of hydraulic conductivity and its role on the dispersion process, *Water Resour. Res.*, *22*, 2069–2082, doi:10.1029/WR022i013p02069.

Zhang, Y., and D. A. Benson (2008), Lagrangian simulation of multidimensional anomalous transport at the MADE site, *Geophys. Res. Lett.*, *35*, L07403, doi:10.1029/2008GL033222.

Zheng, C. (2006), Accounting for aquifer heterogeneity in solute transport modeling: A case study from the Macrodispersion Experiment (MADE) site in Columbus, Mississippi, in *Handbook of Groundwater Engineering*, 2nd ed., edited by J. W. Delleur, pp. 26-1–26-19, CRC Press, Boca Raton, Fla.

Zheng, C., and G. D. Bennett (2002), *Applied Contaminant Transport Modeling*, 2nd ed., 621 pp., John Wiley, New York.

Zheng, C., and S. M. Gorelick (2003), Analysis of the effect of decimeter-scale preferential flow paths on solute transport, *Ground Water*, *41*(2), 142–155, doi:10.1111/j.1745-6584.2003.tb02578.x.

Zheng, C., and J. J. Jiao (1998), Numerical simulation of tracer tests in a heterogeneous aquifer, *J. Environ. Eng.*, *124*(6), 510–516, doi:10.1061/(ASCE)0733-9372(1998)124:6(510).

Zheng, C., and P. P. Wang (1999), MT3DMS: Documentation and user's guide, *Contract Rep. SERDP-99-1*, U.S. Army Eng. Res. and Dev. Cent., Vicksburg, Miss.

J. J. Butler Jr. and G. Liu, Kansas Geological Survey, University of Kansas, Lawrence, KS 66047, USA. (gliu@kgs.ku.edu)

S. M. Gorelick, Department of Environmental Earth System Science, Stanford University, Stanford, CA 94305, USA.

G. R. Tick and C. Zheng, Department of Geological Sciences, University of Alabama, Tuscaloosa, AL 35487, USA.